Supplementary Materials for

Graphene electric field sensor enables single shot label-free imaging of bioelectric potentials

Halleh B. Balch[#,†,‡,§], Allister F. McGuire[#,‖], Jason Horng[#,⊥,†,‡,§], Hsin-Zon Tsai[†], Kevin K. Qi[†], Yi-Shiou Duh[†], Patrick R. Forrester[†], Michael F. Crommie[†,‡,§], Bianxiao Cui[‖], Feng Wang[*,†,‡,§]

Correspondence to: fengwang76@berkeley.edu

Table of Contents

Methods 2
- Prism Fabrication 2
- Description of the Critically Coupled Waveguide 3
- Optical Setup 5
- Data Acquisition 6
- Voltage Sensitivity 7
- Spatial Resolution and Spatio-Voltaic Resolution 8
- Data Analysis 9

Biological Preparation and Measurements 10
- Embryonic Chicken Cardiac Tissue Dissection 10
- Electrophysiology Recordings from Chicken Cardiac Tissue 11
- Contraction Decoupling via Blebbistatin 12
- Multi-electrode Array Measurements 13
- Gate-dependent Measurements of Cardiac Extracellular Potentials 14
- Waveform Polarity Description of the CAGE Sensor 15

Supplemental References 16

Methods

I. Prism Fabrication

The CAGE structure is formed of a prism-coupled slab waveguide coated on one side by large-area monolayer graphene. The structure was designed using a custom Python simulation[1] and fabricated by Edmund Optics. The waveguide consists of a coupling layer of 1000 nm SiO_2 and a waveguide layer of 150 nm Ta_2O_5 deposited via ion-assisted deposition on one face of an SF-11 glass prism. Large-area graphene is grown by chemical vapor deposition (CVD) on copper foil (backside graphene on copper foil was removed via reactive ion etching using 100W O_2 plasma for 45 seconds) and transferred to the surface of the Ta_2O_5 waveguide layer using a standard poly(methyl methacrylate) (PMMA)-supported transfer or a Poly(bisphenol A carbonate) (PC)/PMMA bilayer scaffold[2]. The PC layer prevents the PMMA surface from contacting the graphene surface directly, resulting in less polymer residue. The PMMA top layer provides mechanical support to maintain the integrity of graphene throughout the transfer process. PC was purchased from Sigma Aldrich (#181625, 45K MW). PC was dissolved in chloroform at 3% w/v, then spin coated on the graphene at 3000 rpm for 60 seconds. This was followed by a second spin coat of PMMA (MicroChem, 4% in Anisole by weight. 495K MW) at 3000 rpm for 60 seconds. The copper substrate was etched overnight in 0.1 M ammonium persulfate. The transfer stack was washed in deionized water and transferred to the waveguide surface. The device was air dried and placed at an angle in a desiccator. The device was developed in chloroform to remove the PC/PMMA scaffold, then rinsed with deionized water, acetone, and isopropyl alcohol. The high-quality CVD graphene is monolayer and continuous throughout, producing near-uniform optical absorption at the device/solution interface.

Electrodes formed of Pt (2 nm)/Au (60 nm) are deposited on the graphene surface using a no-contact shadow mask. The electrodes are insulated with nitrocellulose lacquer to prevent adverse oxidative reactions at the aqueous/Au interface during measurements. The CAGE device is mounted in a custom 3D printed holder (Formlabs, Form 2) which permits access to and imaging of the device and sample from both above and below.

II. Description of the Critically Coupled Waveguide

As described above, the complete device consists of a multilayered stack of SF11/SiO_2/Ta_2O_5/graphene/solution that together forms a waveguide that can be critically coupled when an electrostatic potential is applied to the graphene monolayer. To describe the interaction of light with the multilayer device, we consider the stack as comprised of two functional elements, which each form a highly reflective surface: (1) the SF11/SiO_2/ Ta_2O_5 stack and (2) the Ta_2O_5/Graphene/Solution stack (Figure S1).

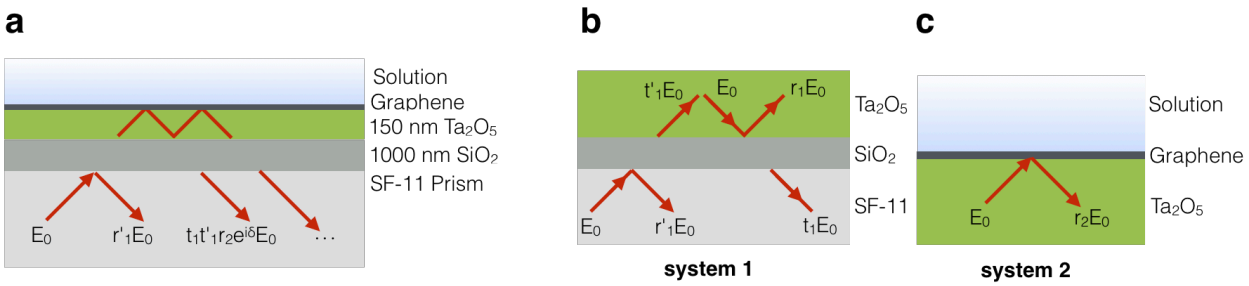

Figure S1 | Details of the critically coupled waveguide structure. a) The multilayered structure (not shown to scale) with the multiple reflections represented by the red arrows. b) The two element stacks comprised of (1) the SF11/SiO_2/Ta_2O_5 stack and (2) the Ta_2O_5/Graphene/Solution stack.

The first element stack (SF11/SiO_2/Ta_2O_5) can be described in context of frustrated total internal reflection, where the coefficients of transmission and reflection from SF11 are t_1' and r_1' and the coefficients at Ta_2O_5 are t_1 and r_1, respectively. From the Fresnel equations, $r_1 = r_1'$ and $t_1 t_1' = (1 - |r_1|^2)e^{(\delta_1 + \delta_1' + \pi)}$, where δ_1 and δ_1' describes the phase of r_1 and r_1', respectively.[3]

The second element stack is composed of Ta_2O_5/Graphene/Solution. In this stack, the reflection coefficient for light incident from the Ta_2O_5 side of the interface is r_2. We calculate $r_2$using the Fresnel relations and through the use of perturbation theory for graphene's absorption: $r_2 = 1 - A_{gr} \times Re[\frac{(1+r_0)^2}{r_0}] = 1 - A_{gr} \times 1.66$. Graphene's absorption is given by A_{gr} and r_0 is the reflection coefficient at the interface of Ta_2O_5/solution in the absence of graphene.

These two element stacks each form a highly reflective interface and together, we can treat the optical cavity formed by these two interfaces as a Fabry-Perot cavity. The total reflected radiation, E_r, is dependent on the interference of multiple reflections within the reflective cavity. Relating the reflection and transmission coefficients, the total reflected radiation can be simplified to: $\frac{E_r}{E_0} = e^{i\delta}\frac{|r_1| - |r_2|e^{i\Delta}}{1-|r_1||r_2|e^{i\Delta}}$ where $\Delta = (\delta + \delta_1 + \delta_2 + \ldots)$ is the round-trip phase accumulation in the waveguide. The resonance condition of the Fabry-Perot cavity takes place under constructive phase accumulation (i.e. $e^{i\Delta}$=1), where the total phase accumulation, Δ,

depends sensitively on the angle of the incident beam coupled into the waveguide structure. Squaring the total reflected radiation, we obtain the reflectance from the waveguide $R = (\frac{|r_1| - |r_2|}{1-|r_1||r_2|})^2$, as shown in the main text. Because graphene's absorption can be varied by an electrostatic gate, the value of $|r_2|$ can be varied *in situ* (Figure S2) .

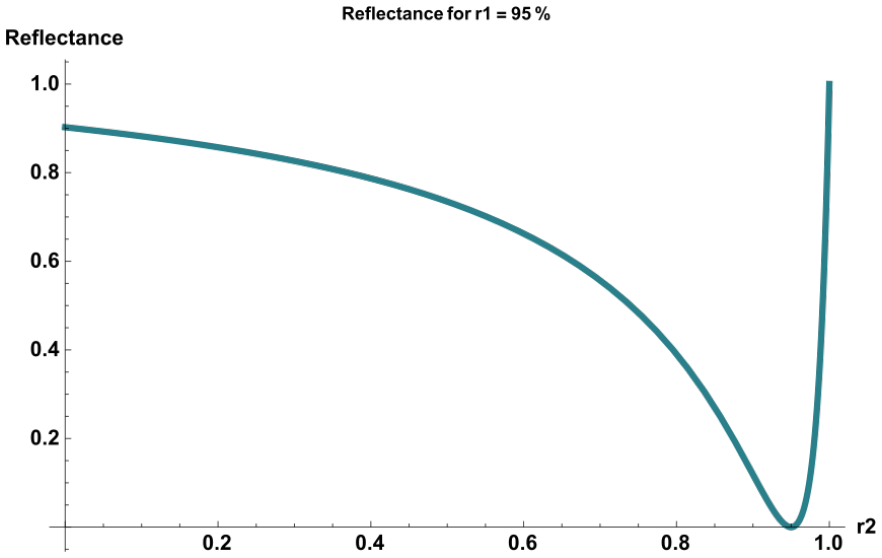

Figure S2 | Simulated total reflectance from the device as a function of r2. For a simulated r1 = 95%, critical coupling takes place when r1=r2, where the total reflectance goes to zero.

At critical coupling, $|r_1| = |r_2|$, and the incident light has near-100% absorption by graphene over the propagation distance in the waveguide (R→0). We operate the device close to the critical coupling condition, where the background reflection is close to zero and small changes to the local gating of graphene result in large changes to the light reflected due to the strongly enhanced light-matter interaction.

III. Optical Setup

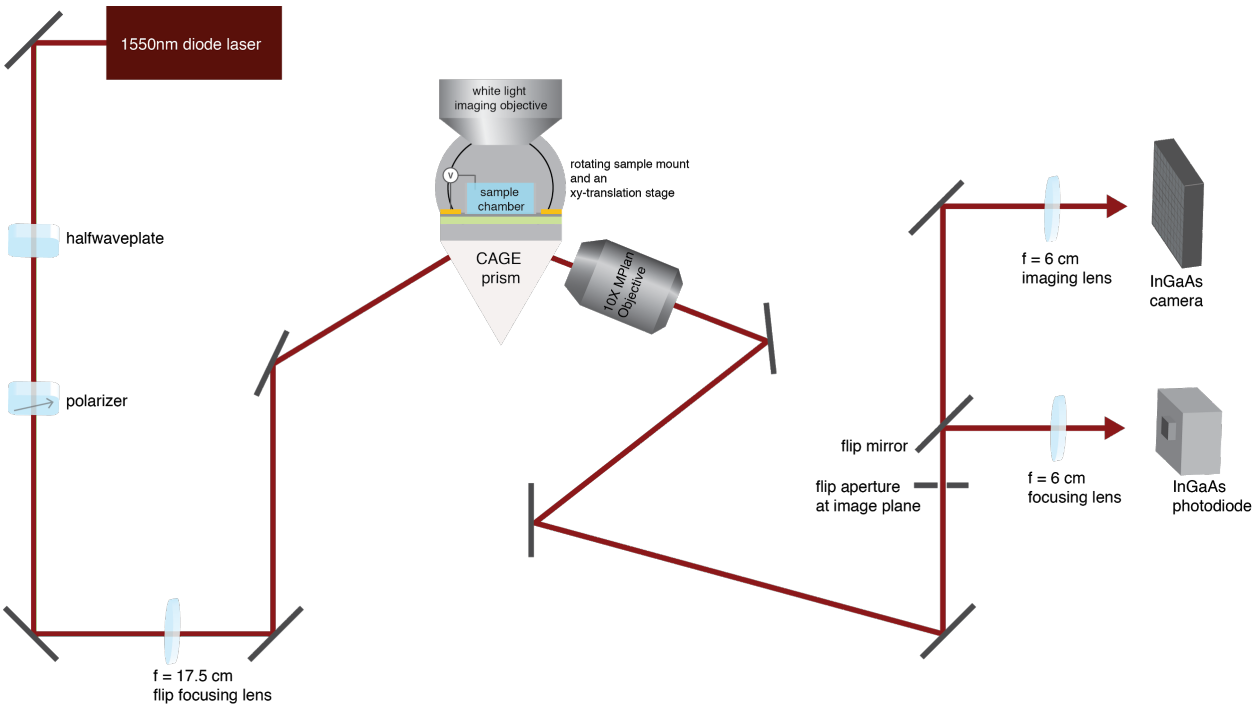

Figure S3 | Schematic of the optical setup.

A stable, 1.55 µm, 15 mW laser beam is generated by a butterfly telecom laser (Newport Model 708 8-Channel Butterfly) with current and temperature controlled by a modular controller (Newport Model 9016). We fix the incident polarization in the TE-direction using a half-wave plate and further clean the incident beam with a calcite polarizer. The incident beam couples into the waveguide from one side of the prism. The incident beam is collimated before coupling into the waveguide. The waveguide-coated prism is mounted to an X-Y translation stage and a rotation stage, which together allow the incident coupling angle to be tuned and the spatial position on the surface of the device to be selected. The signal is out-coupled from the far side of the prism and collected by a 10X MPlan objective or a large lens and sent into an InGaAs two-dimensional camera (Allied Vision Technologies Goldeye 008 SWIR), or into a low-noise InGaAs photodetector, respectively. A set of 5X, 10X, and 20X long working-distance objectives (Mitutoyo) mounted above the sample chamber enables simultaneous white light imaging. Figure S3 illustrates the optical set-up.

IV. Data Acquisition

Each sensor is calibrated to obtain the critical coupling condition prior to measurement. The critical coupling condition is set through shifting the Fermi energy of graphene via an external Ag/AgCl pellet electrode (Warner Instruments) as illustrated in Figure 1d.

Data shown in Figure 2b of the main text were obtained in a saline solution 155 mM NaCl, 2.966 mM Na2HPO4, 1.0588 mM KH_2PO_4. The critical coupling condition was obtained via an external gate voltage Vg = 0.47 V applied through the Ag/AgCl electrode in solution.

Spatially-resolved data shown in 2c were obtained in 1 mgL^{-1} 1 NaCl dissolved in H_2O to more clearly resolve the decaying signal with the camera's 80 Hz frame rate. For spatially-resolved data, the Ag/AgCl electrode was replaced with a parylene-coated Pt/Ir microelectrode tip (World Precision Instruments, #PTM23B05KTH) with a 2 μm radius to form a well-defined electric field distribution. Due to the high impedance at the electrode/solution interface, a higher (1.1V) gate voltage is required at the electrode to produce the same voltage bias and critical coupling condition at the sensor surface (graphene/solution interface). A 10 mV electrical pulse at the microelectrode correspondingly generates a 1.8 mV local field at the graphene/solution interface beneath the microelectrode tip. This modulation is captured in the frames in Figure 3c.

All biological data were obtained in Tyrode's solution (137 mM NaCl, 2.7 mM KCl, 1 mM $MgCl_2$, 1.8 mM $CaCl_2$, 0.2 mM Na_2HPO_4, 12 mM $NaHCO_3$, 5.5 mM D-glucose), warmed to 37 ^oC. 2D spatially-resolved biological data was acquired with an InGaAs two-dimensional camera (Allied Vision Technologies Goldeye 008 SWIR) operated in high speed mode, with 186 fps to obtain the requisite temporal resolution to resolve extracellular potentials (~ 5 ms). To obtain the high speed mode, the camera is operated in an SDK configuration described below. The Goldeye G-008 camera is interfaced to a desktop computer via a highspeed ethernet cable to a gigE CT card. We used two secondary software through Vimba SDK, which includes Vimba Viewer, and Streampix 7 from Norpix, to record high-frame rate videos (Figure 4c). When recording, the feature setting "High speed mode" must be set to "true" and the parameter, "Height", was manually set to Height = 160.

V. Voltage Sensitivity

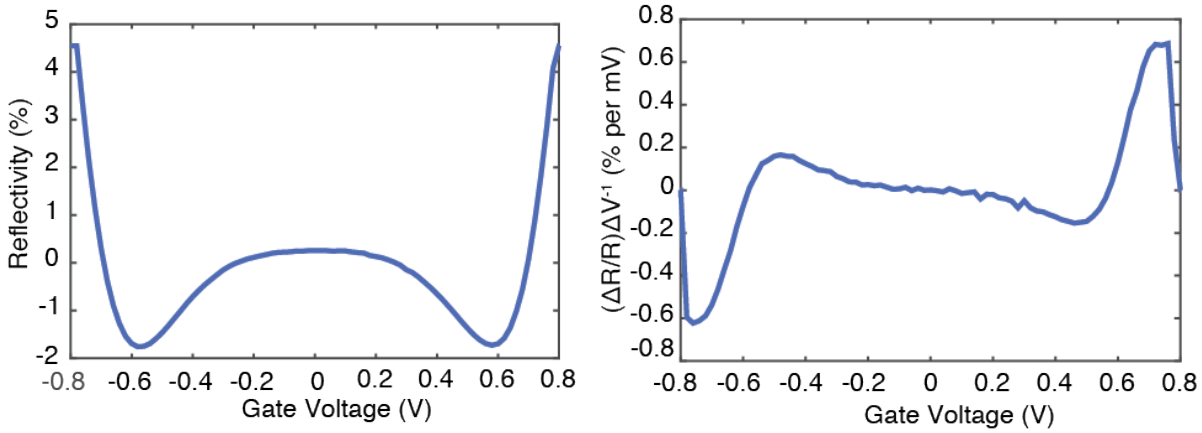

Figure S4 | Optical response of the CAGE sensor and voltage sensitivity. a) Gate-dependent optical reflectivity obtained during a cyclic voltammogram (CV) from -800 mV to +800 mV. The minima in the reflectivity spectra around +/- 600 mV take place at the critical coupling condition. b) The voltage sensitivity, (ΔR/R)/ΔV, is obtained from the CV in (a). This device obtains a maximum voltage sensitivity of 0.68% optical change per mV at V_g = +0.75 mV.

The critical coupling condition is determined through the gate-dependent reflectivity response of the CAGE sensor (SI Figure S4a). The critical coupling condition, $|r_1| = |r_2|$, coincides with the minima of the total Reflectivity, R, and is observed at Vg= +600 mV (electron doped) and Vg= –600 mV (hole doped). As carrier doping in graphene increases, the graphene absorption decreases such that $|r_1| < |r_2|$, as is observed in the increase in total reflectivity away from critical coupling. The voltage sensitivity of CAGE detection, $(\Delta R/R)\Delta V^{-1}$, is characterized by the relative change in reflectivity $(\Delta R/R)$ initiated by a local field potential (ΔV). In SI S.V-b, the voltage sensitivity, $(\Delta R/R)\Delta V^{-1}$, is calculated directly from Figure S.V-a as a function of gate voltage.

The sensor achieves the highest sensitivity close to the critical coupling condition, where the reflection contrast per millivolt is maximized at$(\Delta R/R)\Delta V^{-1}$= 0.68% change in reflectivity per millivolt. In contrast, without the optical amplification provided by the CAGE sensor, graphene produces ~0.005% change in reflectivity per millivolt[1]. The noise level of ~0.02% is due to fluctuations of the laser intensity and optomechanical vibrations.

VI. Spatial Resolution and Spatio-Voltaic Resolution

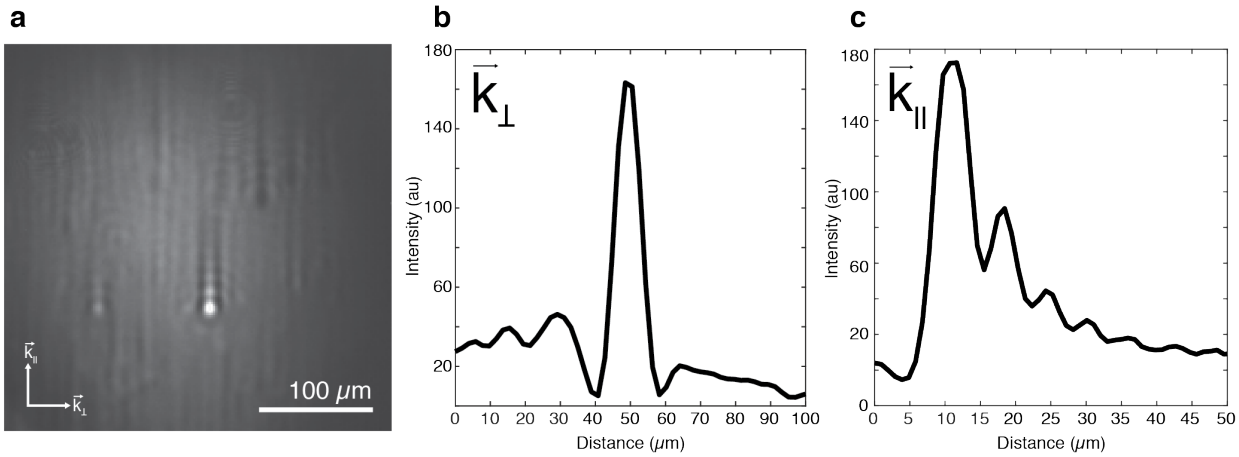

Figure S5 | Spatial resolution calibration in CAGE imaging. a) 2D CAGE image of a 1 µm polystyrene microsphere taken with the CAGE sensor on an InGaAs 2D array. The microsphere is below the b) Line cut of (a) in the direction perpendicular to the direction of light propagation, $\vec{k}$. The spatial resolution, given by the FWHM is ~ 10 µm. c) Line cut of (a) in the direction parallel to $\vec{k}$. The long tail present in the $\overrightarrow{k_{||}}$ direction is due to the reflection decay across the propagation distance of the waveguide. The oscillatory peaks are due to interference effects caused by the angle-dependent reflection coefficient of the waveguide and the finite angular spread of the incident beam. The spatial resolution in this direction is ~ 15 µm.

Spatio-voltaic Resolution

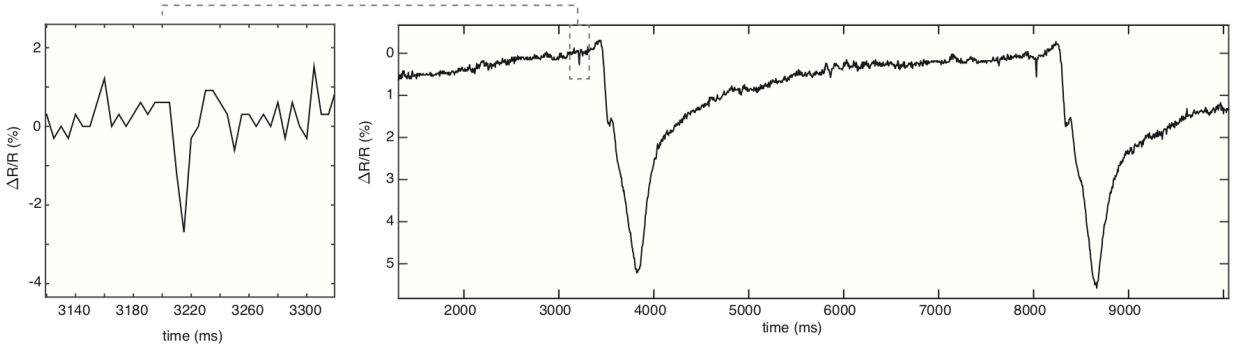

Figure S6 | Spatio-voltaic resolution of CAGE imaging. Extracellular potential from a 21 µm x 42 µm area of raw CAGE data shown in Figure 4d of the main text. Left inset shows the electrical signal with a signal-to-noise ratio of > 2. In CAGE imaging mode, the relatively slow frame rate and limited dynamic range of the InGaAs CCD array can cause blurring due to the action potential dynamics.

VII. Data Analysis

Data were analyzed using a custom MATLAB script. For spatially resolved CAGE images, raw frames were acquired at 186 fps by the InGaAs 2D camera (Allied Vision Technologies Goldeye 008 SWIR) interfaced to a standard desktop via a highspeed ethernet cable to a gigE CT card to accommodate the high data rate as described under Data Acquisition. Raw data was directly loaded into the custom MATLAB script which subtracts a baseline frame at zero signal from all images. By binning the pixels within the 2D array, time series traces are plotted for defined regions of interest across the image plane. The CAGE imaging data is calibrated through $signal(t, pixel\ A) = \frac{R(\ t, pixel\ A) - R(\ t=0, pixel\ A)}{R(\ t=0, pixel\ A)} * voltage\ sensitivity(\frac{\Delta V}{\Delta R/R})$. The spatial calibration for the CAGE image is obtained using a fiducial prism and defines the 0.07 pixels/μm calibration for the CAGE image field and 1.55 pixels/μm in the white light imaging. Defining a bin area of 7 pixels obtains 100 μm spatial resolution across the image plane, corresponding approximately to the size of a single cardiomyocyte cell. 2D figures are plotted sequentially as individual frames. Voltage calibration is set by the responsivity of the specific prism near critical coupling.

Biological Preparation and Measurements

VIII. Embryonic Chicken Cardiac Tissue Dissection

Fertilized white Leghorn chicken eggs (Charles River Laboratories International, Inc.) were incubated at 38 ^{o}C, 40-60% humidity (Hovabator Genesis 1588) for 10-15 days. Chicken hearts were dissected on embryonic day 10-15 (E10-E15) as follows. First, the chick body was removed from the egg to a Petri dish containing ice cold cardioplegic solution (13.44 mM KCl, 12.6 mM $NaHCO_3$, 280 mM glucose, 34 mM mannitol) and immediately decapitated with a razor blade. Holding the chest upward with blunt tweezers, an incision was made with fine tweezers from pelvis to sternum. The tissue was cut away carefully so that the breastplate was exposed and the rib cage was cut away in the same manner maintaining a superficial depth so as to not damage the heart below. Once the heart was exposed, it was monitored for physical contractions. If contractions were not present, the heart was pressed lightly with blunt tweezers to induce a contraction. The presence of a contraction during this period indicated the viability of the heart. In the absence of contractions, the heart was deemed non-viable. Next, the tissue obscuring the heart was cut away, including the pericardium, and the blood vessels at the top were severed as far from the body of the heart as possible. The heart frequently stopped contracting at this point. The heart was removed to a new Petri dish with ice cold cardioplegic solution.

IX. Electrophysiology Recordings from Chicken Cardiac Tissue

Immediately after dissection, the chicken cardiac tissue was transferred to a planar multielectrode array (60MEA200/30iR-Ti, Multi Channel Systems MCS GmbH) seated in a 60-channel amplifier (MEA1060-Inv-BC, Multi Channel Systems MCS GmbH). In the culture well, the tissue was held in place by a nylon mesh (Warner Instruments) lightly compressed from above by a capillary tube in order to ensure a tight seal between the tissue and recording surface. The subsequent addition of Tyrode's solution (137 mM NaCl, 2.7 mM KCl, 1 mM $MgCl_2$, 1.8 mM $CaCl_2$, 0.2 mM Na_2HPO_4, 12 mM $NaHCO_3$, 5.5 mM D-glucose), warmed to 37 ^oC, induced the heart to resume beating. Field potentials were recorded in Tyrode's solution with a Ag/AgCl pellet electrode (Warner Instruments). The tissue was then placed in an incubator (37 ^oC, 5% CO_2) in Tyrode's solution for 10 minutes before being transferred to a CAGE device where it was again held in place by a nylon mesh and capillary tube. Recordings were made in warm Tyrode's solution with a Ag/AgCl pellet electrode.

X. Contraction Decoupling via Blebbistatin

After baseline measurement, cardiac tissue was placed in the incubator for 10 minutes with 100 μM (-)-blebbistatin (Sigma-Aldrich, Inc.) in Tyrode's solution (20 μL of 5 mM stock blebbistatin in DMSO added to 1 mL Tyrode's solution). The tissue was then placed in a multielectrode array in drug-free Tyrode's solution for measurements. When the tissue was moved to the CAGE prism, the IR camera showed reduced, but not completely abolished, contractions. Therefore, blebbistatin was added to the prism chamber itself at 200 μM concentration and the contraction was monitored via the IR camera until it ceased entirely. The solution was replaced with drug-free Tyrode's solution. Optical CAGE measurements were made thereafter.

XI. Multi-electrode Array Measurements

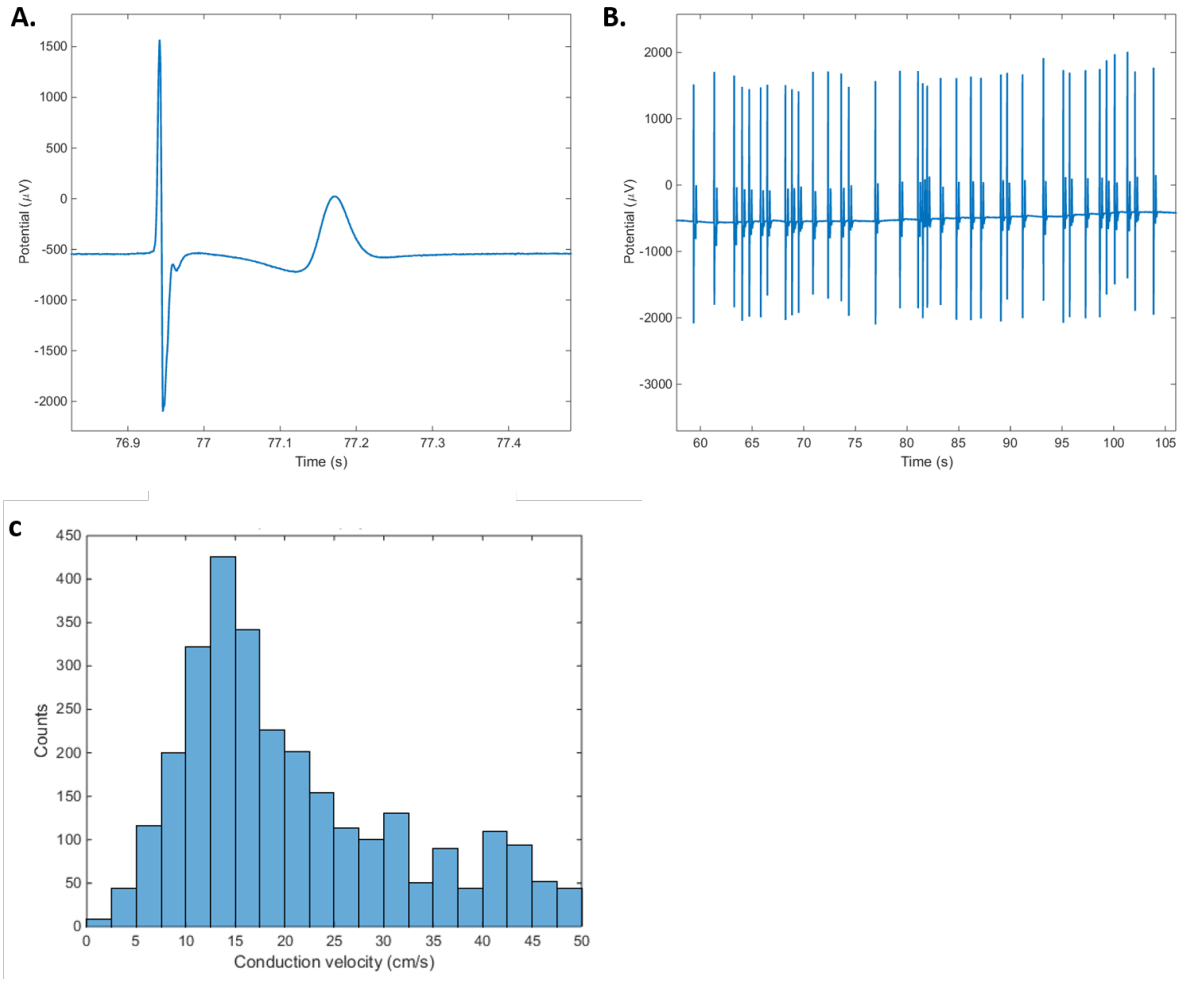

Figure S7 | E15 cardiac tissue field potentials recorded by planar multielectrode array. (a) A single field potential recorded by a 30 µm x 30 µm electrode against a Ag/AgCl reference electrode. (b) Multiple consecutive potentials. (c) Histogram of embryonic chicken heart conduction velocity calculated pairwise across the 60 electrode array.

XII. Gate-dependent Measurements of Cardiac Extracellular Potentials

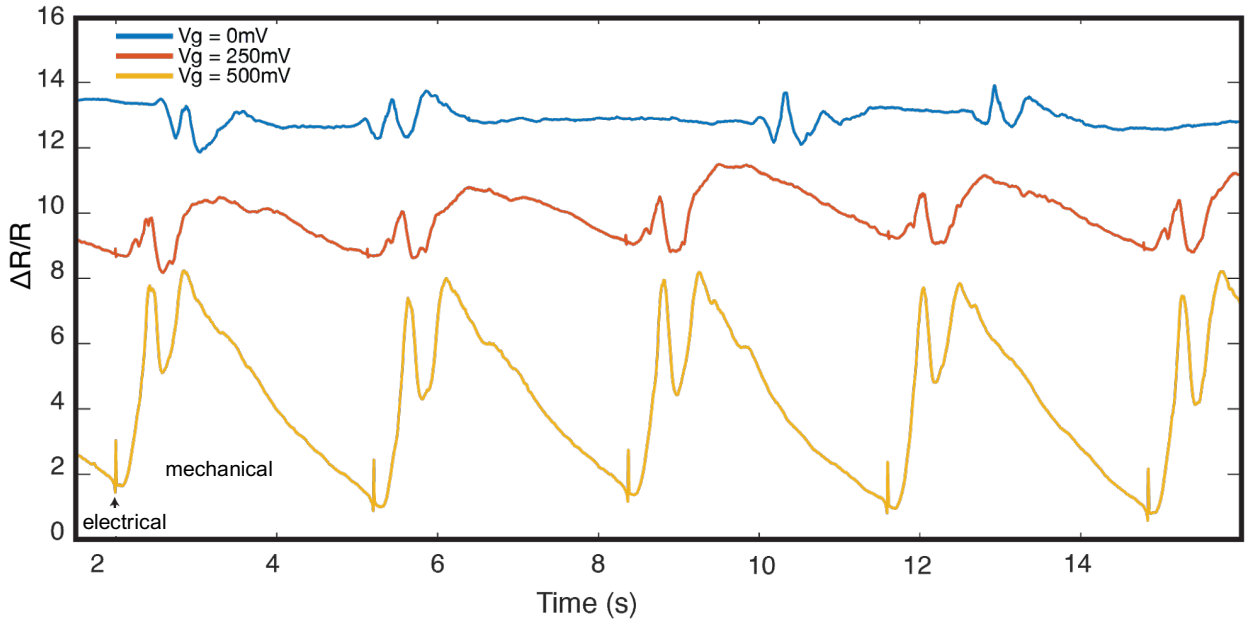

Figure S8 | Supplementary gate-dependence measurements of the cardiac extracellular potentials with both electrical and mechanical signals.

XIII. Waveform Polarity Description of the CAGE Sensor

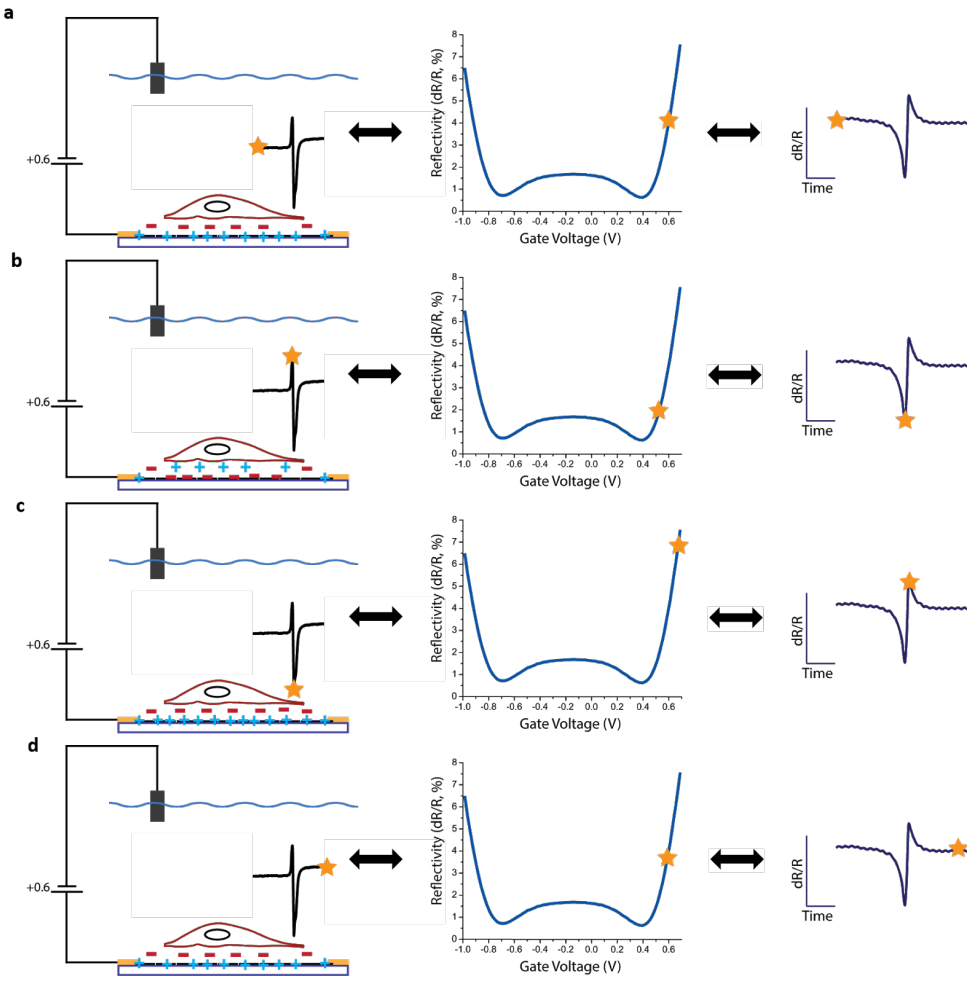

Figure S9 | Detailed Description of Relationship between Field Potential and Graphene Signal. a) The resting membrane potential is enforced by a greater concentration of negative ions outside the cell (red, left diagram) compared to the interior. The initial reflectivity response (right plot) is determined by critical coupling condition of the sensor in the absence of an action potential. b) When the cell fires an action potential, it rearranges the balance of ions, initially creating a relatively positive environment outside the cell (star, left diagram) and yielding a relatively negative compensating charge at the patch of graphene local to the field potential. This modulates the gate voltage (center plot), decreasing the reflectivity (star, right plot). c) The latter portion of the field potential (star, left diagram) again rearranges the balance of ions, yielding a greater concentration of negative ions outside the cell compared to steady state, further gating the graphene in the positive regime (center plot), increasing the reflectivity (star, right plot). d) Finally, after the action potential, steady state resumes and the reflectivity regains its baseline (star, right plot).

Supplemental References

1. Horng, J. *et al.* Imaging electric field dynamics with graphene optoelectronics. *Nat. Commun.* **7**, 13704 (2016).
2. Wood, J. D. *et al.* Annealing free, clean graphene transfer using alternative polymer scaffolds. *Nanotechnology* **26**, 055302 (2015).
3. Zhu, S., Yu, A. W., Hawley, D. & Roy, R. Frustrated total internal reflection: A demonstration and review. *American Journal of Physics* vol. 54 601–607 (1986).